



Supplementary Information for

Phonon Coupling and Transport in Individual Polyethylene Chains: A Comparison Study with the Bulk Crystal

www.rsc.org/

Xinjiang Wang^a, Massoud Kaviani^b and Baoling Huang^{a,*}

In this supplementary document, the basic definition of harmonic and anharmonic force constants are first defined. Then the expressions of symmetry constraints on the harmonic force constants are exemplified, followed by an illustration of the influence of symmetry constraints on the dispersion relation. The lattice constants and the full-range dispersion of PE are also given for a deeper insight of the lattice dynamics results. The thermal expansion coefficients of the bulk PE are calculated at different temperatures to support the ability of the first-principles calculation in recovering the anharmonic properties. Finally, the convergence of both the bulk crystal and the single-chain PE are carefully verified with the supercell size, the mesh size, and different approximations for the Dirac delta function.

Lattice dynamics calculations

Upon expanding the total lattice potential energy E to the third order, the harmonic (Φ) and cubic anharmonic force constants (Ψ) are derivatives of E with respect to the atomic displacement U

$$\Phi_{lb,l'b'}^{ij} = \frac{\partial^2 E}{\partial U_{lb}^i \partial U_{l'b'}^j}, \quad (S1)$$

$$\Psi_{lb,l'b',l''b''}^{ijk} = \frac{\partial^3 E}{\partial U_{lb}^i \partial U_{l'b'}^j \partial U_{l''b''}^k}, \quad (S2)$$

where l and b are the indices of supercell and the atom inside a unitcell and i, j, k are Cartesian indices. Both Φ and Ψ can be calculated with the finite displacement method by replacing the partial derivative operators with small finite displacement in Eqs. (S1) and (S2), and E can be accurately predicted using the first-principles method.

Under the harmonic approximation, the lattice vibrational dynamical matrix is obtained from the harmonic interatomic force constants

$$D_{bb'}^{ij}(\mathbf{q}) = (m_b m_{b'})^{-1/2} \sum_l \Phi_{0b,l'b'}^{ij} e^{i\mathbf{q} \cdot \mathbf{R}_{0b}^{l'b'}} \quad (S3)$$

where \mathbf{q} is the wavevector, $\mathbf{R}_{0b}^{l'b'}$ is distance between two atoms. The phonon frequency ω and eigenvector \mathbf{e} are obtained by diagonalizing the dynamical matrix $\mathbf{D}(\mathbf{q})\mathbf{e}(\mathbf{q}p) = \omega^2(\mathbf{q}p)\mathbf{e}(\mathbf{q}p)$, where p is the phonon polarization index and each wavevector \mathbf{q} and polarization p define a phonon mode λ . The equilibrium phonon Bose-Einstein occupancy is $n_\lambda^o = [\exp(\hbar\omega / (k_B T)) - 1]^{-1}$.

Symmetry constraints on interatomic force constants

The symmetry constraints on both harmonic and anharmonic force constants include the permutational, translational, rotational invariances and point group symmetries¹. In detail, these symmetry constraints, taking Φ for example, are written as the following:

invariance under any interchange of two indices

$$\Phi_{ij}(lb, l'b') = \Phi_{ji}(l'b', lb), \quad (S4)$$

zero force on each atom with any infinitesimal translation of the whole lattice

$$\sum_{l'b'} \Phi_{ij}(lb, l'b') = 0, \quad (S5)$$

zero force on each atom with any infinitesimal rotation of the whole lattice

^a Department of Mechanical and Aerospace Engineering, The Hong Kong University of Science and Technology, Clear Water Bay, Kowloon, Hong Kong. Email address: mebhuan@ust.hk

^b Department of Mechanical Engineering, University of Michigan, Ann Arbor, MI 48109, USA

$$\sum_{l'b'} \Phi_{ij}(0b, l'b') R_k(0b, l'b') - \Phi_{ik}(0b, l'b') R_j(0b, l'b') = 0, \quad (S6)$$

zero torque on each atom with any infinitesimal rotation of the whole lattice

$$\sum_{l'b'} \Phi_{ij}(0b, l'b') R_k(0b, l'b') R_l(0b, l'b') - \sum_{l'b'} \Phi_{kl}(0b, l'b') R_i(0b, l'b') R_j(0b, l'b') = 0, \quad (S7)$$

and point group and space group symmetries,

$$\Phi_{ij}(M(lb), M(l'b')) = \sum_{l''j''} \Phi_{i''j''}(0b, (l'-l)b') M_{ii''} M_{jj''}, \quad (S8)$$

where M is a rotation matrix (e.g. inversion, reflection or rotation) which would map the whole lattice to itself.

It is noteworthy that Eq. (S7) is also included in the Born-Huang invariance conditions² and yet often neglected in describing the symmetry constraints. Sharing the same origin of stress-free equilibrium condition with Eqs. (S5) and (S6)³, Eq. (S7) is important and the neglect of it would result in finite stress in the chain that could disrupt the dispersion relation at long wavelengths.

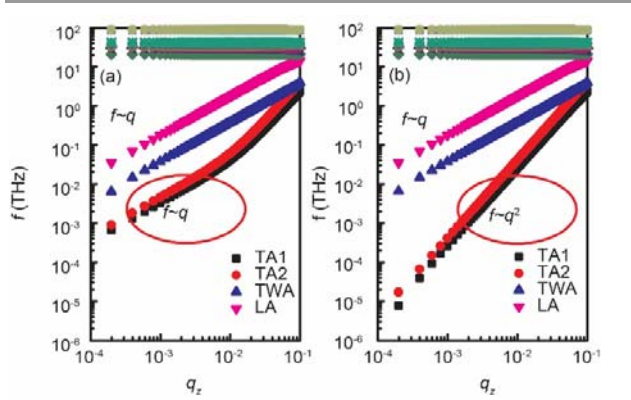


Fig. S1. Dispersion of relation of an individual PE chain (a) before and (b) after exerting the symmetry constraints in the logarithmic scale.

Lattice structure of the bulk PE crystal

The fully relaxed PE crystal has an orthorhombic structure with the parameters a , b and c being the lattice constants and ϑ being the chain setting angle (the dihedral angle between the plane of carbon atoms on a single chain and the xz plane). The predicted lattice parameters are listed and compared with experiments at different temperatures in Table SI, with the maximum deviation less than 2%, verifying the accuracy of the first-principles calculations in predicting the bulk PE crystal structure.

Table SI. Calculated lattice parameters for the bulk PE, in comparison with reported experimental results.

Lattice parameter	Predicted	Exp. (4 K) ⁴	Exp. (10 K) ⁵	Exp. (77 K) ⁶
s				
a (Å)	6.978	7.121	7.16	7.155
b (Å)	4.854	4.851	4.86	4.899
c (Å)	2.553	2.548	2.534	2.547

ϑ (°)	43.3	41 ± 1		
-----------------	------	------------	--	--

Full-range dispersion relation

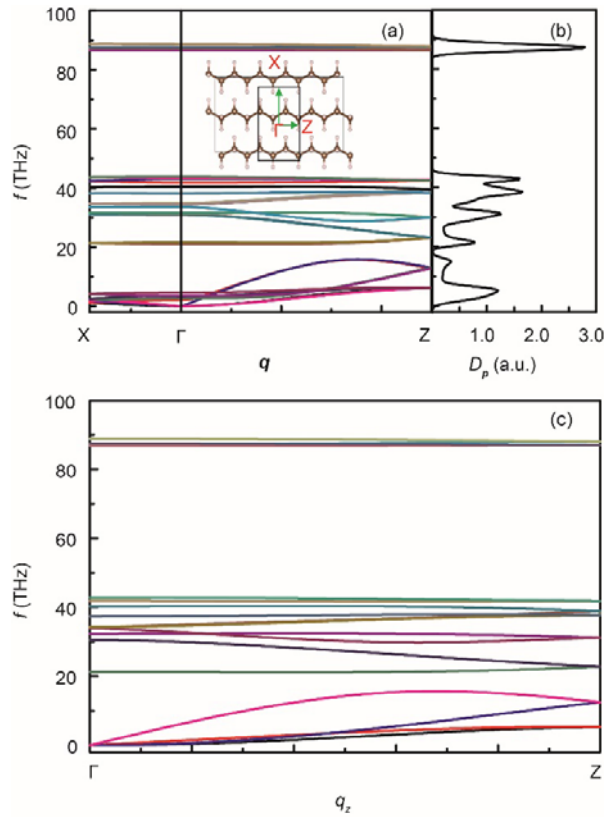


Fig. S2. (a) Predicted phonon dispersion of bulk PE crystal along different directions (b) phonon density of states (D_p) of bulk PE, and (c) phonon dispersion relation of single-chain PE in full range.

Thermal expansion coefficient

To verify the accuracy of the potentials used in predicting the anharmonic properties, the predicted thermal expansion (α) of the PE crystal is compared with the experiments, since α arises from the anharmonic lattice vibration. This is realized by minimizing the Helmholtz free energy with respect to the lattice parameters. Under the quasi-harmonic approximation (linear relation of phonon frequency change and lattice constants), we have

$$\alpha_i = \frac{1}{N_0 \Omega} \sum_{\lambda} C_v(\lambda) S_{ij} \gamma_j(\lambda), \quad (S9)$$

where S is the compliance tensor, and $\gamma_i = \partial \ln \omega_{\lambda} / \partial \ln a_i$ is the diagonal components of modal Gruneisen tensor, which can be acquired from anharmonic force constants^{7,8}

$$\gamma_{\lambda}^i = -\frac{1}{6\omega_{\lambda}^2} \sum_{1,2} \Psi_{0b,l'b',l'b''}^{ijk} \frac{e^{ik-(l'-l')}}{(M_b M_{b'})^{1/2}} J_{0b}^i (e_{\lambda}^{bj})^* e_{\lambda}^{b'k}. \quad (S10)$$

The anisotropic thermal expansion α is important and derives from the lattice anharmonicity and with high crystallization ratio α varying little with the increase in crystallinity at low temperatures⁹. Therefore, despite the lack of κ data, comparisons of the predicted α with low temperature experiments can help validate the anharmonic potentials used in the κ prediction. Figures S3(a) to (d) show the predicted directional α compared with X-ray experiments^{10–12} for temperatures up to 200 K [higher than the sub-glass transition temperature of high-density polyethylene (~ 145 K)⁹]. The change of directional α with temperature is well captured, especially along the ab plane. The difference in the axial direction [Fig. S3(c)] is rather small at temperatures lower than 100 K (but increases at higher temperatures). The predicted axial α_c is negative at temperatures lower than 200 K (tends to saturate and slightly increase for $T > 150$ K), but measured value decrease over the temperature range, and can be due to the imperfect crystallization of the samples ($\sim 70\%$ in Ref. ¹²). The taut-tie molecules among microcrystals resemble fully crystalline PE in thermal expansion behavior at low temperatures, but lead to contraction of the separation distance of crystallites when tie molecules vibrate with large amplitude. This will result in large negative thermal expansion at temperatures higher than the sub-glass transition point. For ideal crystal, this secondary effect caused by the tie molecules does not exist (the predicted axial thermal expansion is higher than the experiments at around 200 K), but the agreement in general is good.

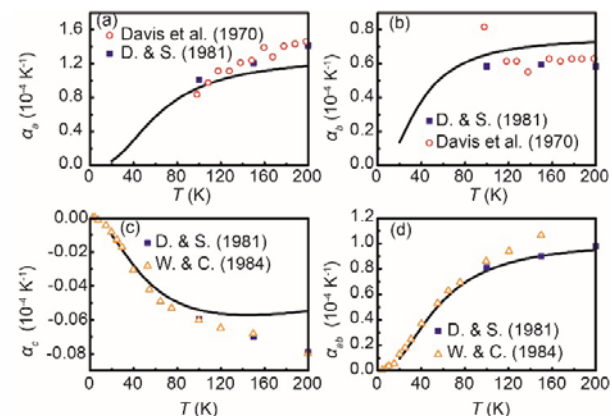


Fig. S3. The variations of predicted anisotropic thermal expansion coefficient with temperatures along axis (a) a , (b) b , and (c) c , and (d) plane ab , and compared with experimental studies from Davis et al. (1970)¹¹, Dadobaev and Slutsker (1981)¹⁰ and White and Choy (1984)¹².

Convergence test for thermal conductivity (bulk PE)

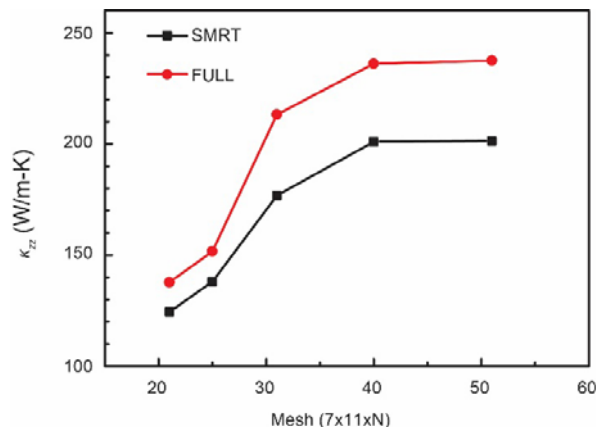


Fig. S4. Convergence of axial thermal conductivity at room temperature of bulk PE in regards to mesh size. Both results of full solution of BTE with the conjugate-gradient method and the solution with the single-mode relaxation time (SMRT) approximation are shown.

Figure S4 shows the variation of calculated axial thermal conductivity of bulk PE at room temperature with different mesh size in the chain direction. All the calculations of bulk PE reached the given criterion (relative κ error $< 10^{-7}$) in CG iterations within around 50 steps.

Convergence test for supercell size (chain PE)

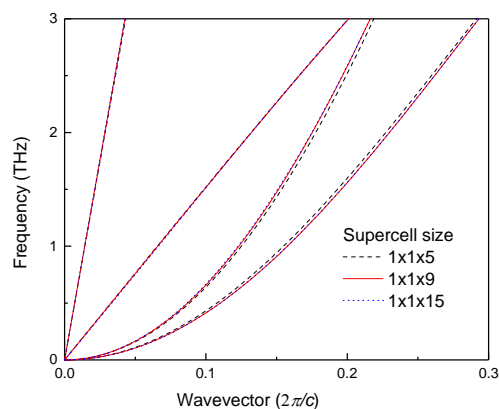


Fig. S5. The dispersion relation for 1-D PE chain along Γ to Z direction.

The influence of the supercell size on both the harmonic and anharmonic force-constant calculations has been carefully tested. The tests for the harmonic force constants are based on the trends in the dispersion relation changes. As Fig. S5 shows, the harmonic dispersion relation calculated from the $1 \times 1 \times 9$ supercell resembles that from $1 \times 1 \times 15$, thus considered to be adequate for the lattice dynamics calculations.

As for the anharmonic force constants, the cost for each expansion is much higher and thus not feasible. Alternatively, through

analyzing the force constant-distance behavior, we conclude that the anharmonic force constants have a decreasing trend which is a major index for physicality verification. The maximum interacting distance reaches 7 Å, almost reaching the van der Waals limit. These are shown in Fig. S6. At such a limit, the anharmonic force constants are around 3 orders of magnitude lower than the maximum values. Further increase of the supercell hardly increases the accuracy (but results in larger calculation noises). Therefore, we conclude that such an expansion for the anharmonic force constants suffices as well.

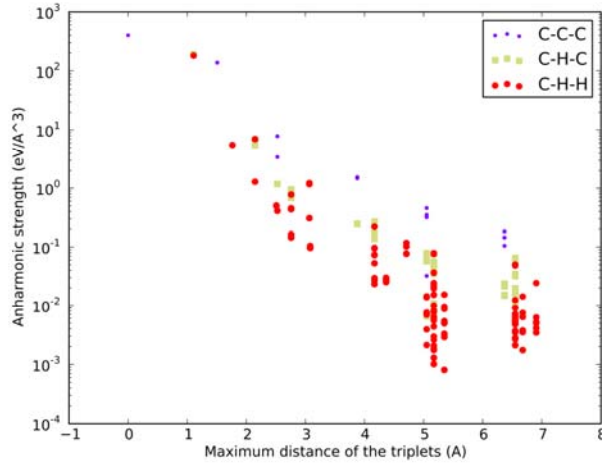


Fig. S6. R^2 norm of anharmonic force-constants with respect to the maximum distance in a triplet of atoms.

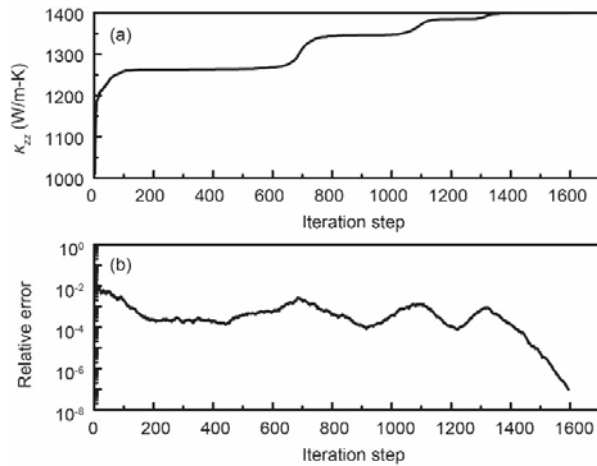


Fig. S7. (a) Thermal conductivity of single-chain PE with the iteration step during the solution of BTE using conjugate gradient technique. (b) Relative error variance with iteration step.

Dirac Delta function estimation

A precise estimation of the phonon-phonon scattering rates entails a proper approximation of the Dirac delta function, which is required to fulfil the energy conservation law during a scattering event¹³. Conventionally, the Dirac delta function is approximated as a Gaussian function with a finite smearing factor σ

$$\delta(\omega - \omega') = (2\pi\sigma^2)^{-1/2} \exp\left(-(\omega - \omega')^2 / (2\sigma^2)\right). \quad (\text{S11})$$

The Dirac delta function appearing in the 3-phonon scattering terms is implemented by fixing ω and varying $\omega \pm \omega''$, which is treated as a single parameter ω' . However, selecting appropriate mesh size and the corresponding smearing factor σ is tricky, and up until now there is no rigorous way to select the appropriate combination, although this is much less challenging for 3-D systems. More importantly, the results of the single PE chain using the Gaussian smearing are found quite sensitive to the choice of the smearing factor even at a large mesh size. So we developed the hyperspace tetrahedron method based on the linear tetrahedron method^{14,15} for the Dirac delta function.

In the linear tetrahedron method, for a 3D system, the Brillouin zone is first meshed to a set of tetrahedrons. Heaviside's step function $H(\omega)$ is calculated by calculating the filled volume in each tetrahedron and then the Dirac delta function is obtained by differentiating H in regard to ω . It is known for its dependence with only the mesh size and the ability to approximate the Dirac delta function even at a relatively small mesh size without significantly impairing the accuracy¹⁶. As to a 1-D Brillouin zone as that of the single-chain PE, starting from Ref.¹⁵, the estimation of $\delta(\omega - \omega_q)$ is

$$\delta(\omega - \omega_q) = \sum_{j=1}^2 g_{q,j}(\omega), \quad (\text{S12})$$

where g is evaluated on the \mathbf{q} -point together with its two neighbors indexed by j .

$$g_{q,j} = \begin{cases} \frac{|\omega - \omega_j|}{(\omega_q - \omega_j)^2} & \text{if } \min(\omega_j, \omega_q) < \omega < \max(\omega_j, \omega_q) \\ 0 & \text{else} \end{cases}. \quad (\text{S13})$$

There are some difficulties to apply this method in a 1-D mesh. First, energy conservation may be satisfied intrinsically [i.e., the denominator $\omega_q - \omega_j = 0$ in Eq. (S13)], as illustrated by a collinear scattering event in the three-phonon processes on a linear dispersion relation (e.g., the longitudinal acoustic branch). Then the estimated delta function for 1-D mesh from Eqs. (S12) and (S13) might be infinite, while in a 3-D mesh the chance that the four corners of a tetrahedron have the same frequency is much slimmer. Another problem with the above estimation is its only dependence on the gradient of dispersion relation at \mathbf{q} -point. Therefore, if there is an exchange of integration sequence of \mathbf{q} and \mathbf{q}' in $\iint F_{\mathbf{q},\mathbf{q}'} \delta(\omega_q - \omega_{\mathbf{q}'}) d\mathbf{q}d\mathbf{q}'$, the estimation using the tetrahedron method leads to $\delta(\omega_q - \omega_{\mathbf{q}'}) \neq \delta(\omega_{\mathbf{q}'} - \omega_q)$. Especially, prominent in three-phonon scatterings, the asymmetric delta function breaks the interchangeability of the three phonons in the scattering probability $P_{\lambda,\lambda'}^{\lambda''}$. This would further lead to the breakdown of the positive definite property of the collision matrix¹⁷, which could possibly result in a false divergent thermal conductivity calculation.

This is solved by realizing the double integration and building a hyperspace $\mathbf{q} \otimes \mathbf{q}'$, which is discretized subsequently in this higher dimensional space $(\iint F_{\mathbf{q},\mathbf{q}'} \delta(\omega_q - \omega_{\mathbf{q}'}) d\mathbf{q}d\mathbf{q}' \rightarrow$

$\int_{q \in q'} F_{q,q'} \delta(\omega_q - \omega_{q'}) dS_{q,q'}$). This process theoretically turns the tetrahedron for a single integration in 3-D space into a 6-symplex (a counterpart of tetrahedron in 6-D space). Then the 6-symplex enables interchanging the integration sequence for any two dimensions and thus the Dirac delta function is symmetric again. Evaluation of the delta function would be tedious in the 6-D space, and fortunately the breakdown of asymmetry is not so significant for a 3-D bulk material. For the 1-D PE chain however, the hyperspace is only a 2-D space in which the Dirac delta function is readily and elegantly evaluated.

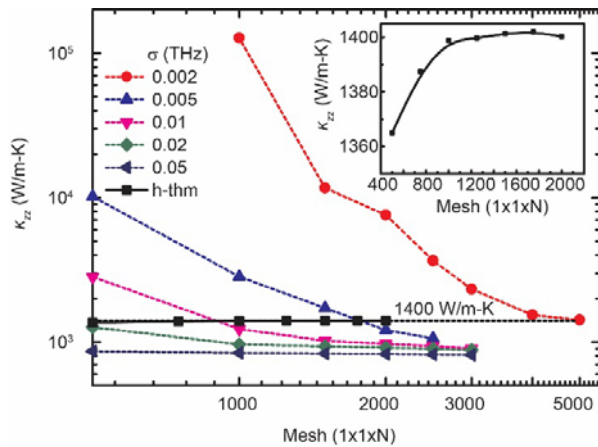


Fig. S8. Convergence test of axial thermal conductivity of single-chain PE with mesh size. Gaussian smearing with different smearing factor (σ) ranging from 0.002 to 0.05 THz are compared with the results using the hyperspace tetrahedron method (h-thm). The inset is a zoom-in illustration of calculated κ with mesh size using the h-thm method.

Fig. S8 compares the influence of different choices of σ on thermal conductivity estimation of the 1-D PE chain. It is observed that large σ values tend to falsely include more scattering events and thus underestimate thermal conductivity while too small σ values at a small mesh size overestimate thermal conductivity. Therefore, the ideal approach is to use an infinitely large mesh size and a smearing factor approaching 0, which is obviously too time consuming. On the contrary, as shown in Fig. S8, κ of single-chain PE using the hyperspace tetrahedron method is quite consistency (error < 0.5%) and reaches the limiting value of Gaussian approximation even at small mesh sizes. The small variance of κ with increasing mesh size indicates convergence with discretization in the Brillouin zone and also validates the applicability of the tetrahedron method in the 1-D PE chain.

REFERENCES

- 1 K. Esfarjani and H. T. Stokes, *Phys. Rev. B*, 2008, **77**, 144112.
- 2 M. Born and K. Huang, *Dynamical Theory of Crystal Lattices*, Clarendon Press, Oxford : New York, 1998.
- 3 R. A. MacDonald, *Phys. Rev. B*, 1972, **5**, 4139.
- 4 G. Avitabile, R. Napolitano, B. Pirozzi, K. D. Rouse, M. W. Thomas and B. T. M. Willis, *J. Polym. Sci. Polym. Lett. Ed.*, 1975, **13**, 351–355.
- 5 M. Shen, W. N. Hansen and P. C. Romo, *J. Chem. Phys.*, 1969, **51**, 425–430.

- 6 P. R. Swan, *J. Polym. Sci.*, 1962, **56**, 403–407.
- 7 K. Esfarjani, G. Chen and H. T. Stokes, *Phys. Rev. B*, 2011, **84**, 085204.
- 8 J. Fabian and P. B. Allen, *Phys. Rev. Lett.*, 1997, **79**, 1885–1888.
- 9 C. L. Choy, F. C. Chen and K. Young, *J. Polym. Sci. Polym. Phys. Ed.*, 1981, **19**, 335–352.
- 10 G. Dadobaev and A. I. Slutsker, *Fiz. Tverd. Tela*, 1981, **23**, 1936–1942.
- 11 G. T. Davis, R. K. Eby and J. P. Colson, *J. Appl. Phys.*, 1970, **41**, 4316–4326.
- 12 G. K. White and C. L. Choy, *J. Polym. Sci. Polym. Phys. Ed.*, 1984, **22**, 835–846.
- 13 D. A. Broido, M. Malorny, G. Birner, N. Mingo and D. A. Stewart, *Appl. Phys. Lett.*, 2007, **91**, 231922.
- 14 A. Togo, L. Chaput and I. Tanaka, *Phys. Rev. B*, 2015, **91**, 094306.
- 15 A. H. MacDonald, S. H. Vosko and P. T. Coleridge, *J. Phys. C Solid State Phys.*, 1979, **12**, 2991.
- 16 P. E. Blöchl, O. Jepsen and O. K. Andersen, *Phys. Rev. B*, 1994, **49**, 16223–16233.
- 17 L. Chaput, *Phys. Rev. Lett.*, 2013, **110**, 265506.